

**Photoassociation driven by a short laser pulse at millikelvin temperature**

Meng Wang, Jing-Lun Li, Xue-Jin Hu, Mao-Du Chen, and Shu-Lin Cong\*

*School of Physics, Dalian University of Technology, Dalian 116024, China*

(Received 16 April 2017; published 20 October 2017)

We investigate theoretically the photoassociation process of  $^{85}\text{Rb}$  atoms driven by a short laser pulse at several millikelvins. At this temperature, the actions of the rotational barrier, weights of initial scattering states, and shape resonance emerge and have an influence on the thermally averaged photoassociation probability. The calculated thermal weighted population distribution of rotational states agrees well with photoassociation spectrum experiment. The thermally averaged photoassociation probability decreases with an increase in temperature.

DOI: [10.1103/PhysRevA.96.043417](https://doi.org/10.1103/PhysRevA.96.043417)**I. INTRODUCTION**

Atomic gases at low and ultralow temperature have attracted much attention from researchers due to their potential applications in quantum information [1–3], fundamental physical constant measurement [4,5], and ultracold chemistry [6]. Photoassociation (PA) and magnetic association are two efficient ways of preparing cold or ultracold molecules. In the magnetic association process, weakly bound molecules are formed by the magnetically tuned Feshbach resonance [7,8]. In the PA process, two atoms are associated into a molecule under the action of a laser field [9–12]. The photoassociation process is directly related to the interaction property of the colliding atomic pair as well as the structure of the molecule being formed [13].

In recent years, with the development of laser cooling and magnetic confinement technologies, many new experimental investigations have been performed to produce cold (1 mK to 1 K) and ultracold ( $< 1$  mK) molecules in atomic gas. Researchers initially mainly utilized continuous laser to realize the photoassociation process [14,15] and then utilized short or ultrashort pulses with a large bandwidth in the frequency domain to improve the photoassociation efficiency [16–24]. Shape resonance is elastic scattering resonance associated with quasibound diatomic states trapped behind a centrifugal barrier [25–29]. Shape resonance plays an important role in the cold-atomic collision process because the collision energy is often lower than the centrifugal barrier. The photoassociation probability can be enhanced by suitably adjusting the shape resonance in the scattering of ground-state atoms because the shape resonance increases the amplitude of the wave function inside the centrifugal barrier. Boesten *et al.* presented a detailed study on shape resonance in cold-atomic scattering [25]. González-Férez *et al.* pointed out that shape resonance can be modulated by using nonresonant light to enhance the photoassociation probability [26].

For a binary collision, temperature is one of the determinant factors in a PA process. With decreasing temperature, higher rotational and vibrational degrees of freedom are partly frozen. In the case of ultralow temperatures, atomic scattering results mainly from  $s$ -wave scattering [30]. Huang *et al.* used a

single  $s$ -wave-scattering wave function to investigate the formation of ultracold  $^{85}\text{Rb}_2$  molecules via photoassociation by two-color laser fields with modulation of the Gaussian amplitude at an ultralow temperature,  $T = 100 \mu\text{K}$  [31]. At higher temperatures, the atomic scattering state can penetrate the rotational barrier easily due to the higher translational kinetic energy. Thus the association process is likely to happen at a short atomic separation [32]. At a finite temperature, the thermal averaged initial state can be described by box-discretized continuum states with a Boltzmann distribution. Koch *et al.* calculated the absolute number of molecules per PA pulse in an initial thermal ensemble of atoms [33]. In the experimental setting, Gardner *et al.* researched collisions of  $^{85}\text{Rb}$  atoms at millikelvin temperatures [34]. They obtained some  $^{85}\text{Rb}$  photoassociation data and calculated the atomic interaction parameters from the fluorescence rotational spectrum.

In the present work, we investigate theoretically the photoassociation process driven by a short laser pulse at millikelvin temperatures. Under this temperature condition, some higher rotational and vibrational degrees of freedom are activated. The rotational barrier, weight, and shape resonance influence the photoassociation probability. Therefore, the initial state should be described using the rotational and translational quantum states with a Boltzmann distribution, instead of a pure  $s$ -wave-scattering state. Because of the larger bandwidth of picosecond laser pulses in the frequency domain and higher temperature, more shape resonances take part in the photoassociation process and influence the photoassociation probability.

The paper is organized as follows: The theoretical approach is reported in Sec. II. The PA process at millikelvin temperatures is described and discussed in Sec. III. The conclusion is drawn in Sec. IV.

**II. THEORETICAL APPROACH**

We consider the photoassociation process in which two cold colliding  $^{85}\text{Rb}$  atoms are associated into a  $\text{Rb}_2$  molecule from the ground electronic  $X^1\Sigma_g^+$  ( $5S + 5S$ ) state to the excited electronic  $0_u^+$  ( $5S + 5P_{1/2}$ ) state by a short laser pulse at several millikelvins, as shown in Fig. 1(a). The  $0_u^+$  ( $5S + 5P_{1/2}$ ) and  $0_u^+$  ( $5S + 5P_{3/2}$ ) states are coupled by

\*shlcong@dlut.edu.cn

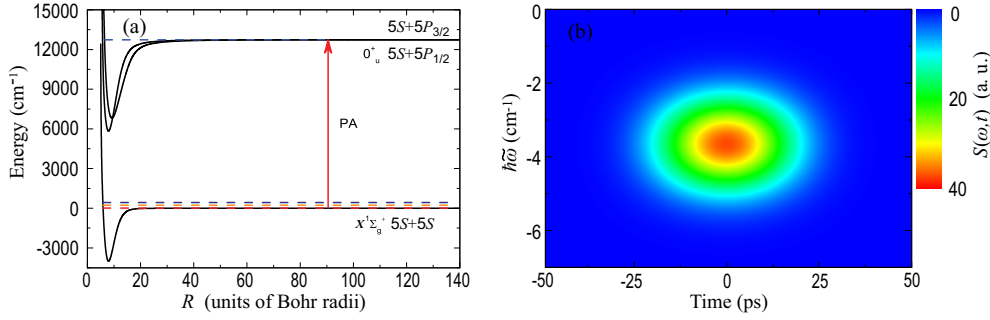


FIG. 1. (a) Schematic of the photoassociation process at millikelvin temperature. The initial state related to the ground electronic  $X^1\Sigma_g^+$  state and high rovibrational level of the excited electronic  $0_u^+$  state (dashed blue line) are coupled by a short laser pulse. Dashed lines just above the  $X^1\Sigma_g^+$  state denote the initial continuum state with a thermal distribution. (b) Time- and frequency-resolved spectra  $S(\omega, t)$  of the laser pulse.  $\hbar\tilde{\omega} \equiv \hbar\omega - E_{D_1}$  denotes the difference between the photon energy  $\hbar\omega$  and the  $5S + 5P_{1/2}$  dissociation limit  $E_{D_1}$  (i.e., the atomic resonance  $D_1$  line).

the spin-orbit interaction. Within the dipole approximation and rotation-wave approximation, the Hamiltonian describing

the photoassociation process can be expressed in the diabatic representation as [31]

$$\hat{\mathbf{H}} = \begin{pmatrix} \hat{T} + \hat{V}_{X^1\Sigma_g^+}(R) + \frac{\hat{L}^2}{2\mu_m R^2} & -\hat{\mu}(R) \cdot \hat{E}(t) & 0 \\ -\hat{\mu}(R) \cdot \hat{E}(t) & \hat{T} + \hat{V}_{A^1\Sigma_u^+}(R) + \frac{\hat{L}_e^2}{2\mu_m R^2} - \hbar\omega(t) & \Delta_{\Pi\Sigma} \\ 0 & \Delta_{\Pi\Sigma} & \hat{T} + \hat{V}_{b^3\Pi_u}(R) + \frac{\hat{L}_e^2}{2\mu_m R^2} - \Delta_{\Pi\Pi} - \hbar\omega(t) \end{pmatrix}, \quad (1)$$

where  $\hat{T}$  is the radial part of the kinetic energy operator,  $R$  the interatomic distance, and  $\mu_m$  the reduced mass.  $\hat{L}$  and  $\hat{L}_e$  are the rotational quantum operators of the ground electronic state and excited electronic state, respectively.  $\Delta_{\Pi\Pi}$  and  $\Delta_{\Pi\Sigma}$  denote the diagonal and off-diagonal spin-orbit couplings, respectively. The interaction  $-\hat{\mu}(R) \cdot \hat{E}(t)$  couples different rotational states, which can be expressed as  $-\frac{1}{2}\mu(R)E_0 f(t)C_{l\pm 1}^l$ , where  $\mu(R)$  is the transition dipole moment,  $E_0$  the amplitude of the electric field, and  $f(t)$  the temporal envelope.  $C_{l\pm 1}^l = \langle P_l | \cos\theta | P_{l\pm 1} \rangle$ , where  $P_l$  and  $P_{l\pm 1}$  are the Legendre polynomial normalized with respect to unity for the ground and excited electronic states, respectively.  $\omega(t)$  is the frequency of the laser pulse. The potential function of the ground electronic  $X^1\Sigma_g^+$  state is adopted from Ref. [35]. The potentials of the excited  $A^1\Sigma_u^+$  and  $b^3\Pi_u$  states and the spin-orbit coupling are taken from Ref. [36]. The  $R$ -dependent transition dipole moment  $\mu(R)$  is obtained from Ref. [37].

The photoassociation dynamics can be studied by solving the time-dependent Schrödinger equation

$$i\hbar \frac{\partial}{\partial t} |\Phi(t)\rangle = \hat{\mathbf{H}}(t) |\Phi(t)\rangle \quad (2)$$

using the mapped Fourier grid Hamiltonian method [38] and Chebychev polynomial propagation method [39,40].

The laser pulse is expressed as  $\tilde{E}(\omega)$  in the frequency domain [41],

$$\tilde{E}(\omega) = A(\omega) e^{-i\phi(\omega)t}, \quad (3)$$

where  $A(\omega) = \exp[-2\ln 2(\omega - \omega_0)^2 / \omega_f^2]$  denotes the spectral amplitude, with  $\omega_f$  being the full width at half-maximum (FWHM).  $\phi(\omega)$  is the spectral phase of the laser pulse. Using the Fourier transform, the electric field  $E(t)$  of the laser pulse

in the time domain is given by

$$E(t) = \frac{1}{2\pi} \int_{-\infty}^{\infty} \tilde{E}(\omega) e^{-i\omega t} d\omega, \quad (4)$$

where  $\tilde{E}(\omega)$  is a complex function containing all the information concerning the laser pulse. The choice of  $\omega_f$  is related to the resonance region in the photoassociation process. The spectral phase  $\phi(\omega)$  plays a major role in the pulse shaping process. The photoassociation process can be optimized by adjusting  $\omega_f$  and  $\phi(\omega)$ . A short laser pulse with a larger bandwidth can cover more rovibrational levels of the excited electronic state and can improve the photoassociation efficiency.

Figure 1(b) shows the time- and frequency-resolved spectrum  $S(\omega, t)$  of the laser pulse used in the present work. This time- and frequency-resolved spectrum well displays the nature of the laser pulse.  $\hbar\tilde{\omega} \equiv \hbar\omega - E_{D_1}$  denotes the difference between the photon energy  $\hbar\omega$  and the  $5S + 5P_{1/2}$  dissociation limit  $E_{D_1}$  (i.e., the atomic resonance  $D_1$  line). The time- and frequency-resolved spectrum of the modulated laser field is given by [42,43]

$$S(\omega, t) = \left| \int_{-\infty}^{\infty} H(t' - t, T_\omega) E(t') e^{i\omega t'} dt' \right|^2, \quad (5)$$

where the Black window function  $H(t' - t, T_\omega)$  is expressed as

$$H(t' - t, T_\omega) = 0.42 + 0.50 \cos \left[ \frac{2\pi}{T_\omega} (t' - t) \right] + 0.08 \cos \left[ \frac{4\pi}{T_\omega} (t' - t) \right] \quad (6)$$

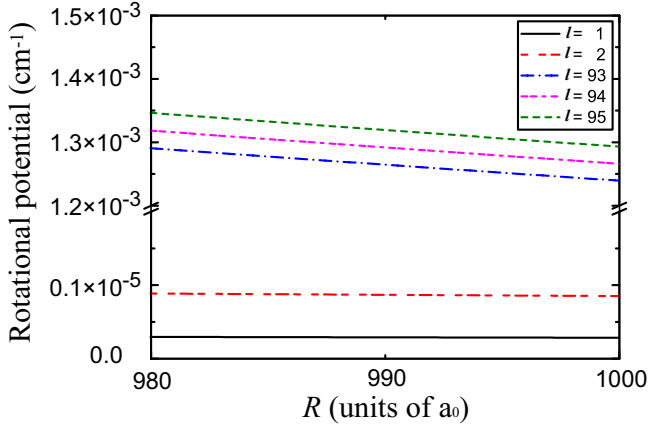


FIG. 2. Rotational potential energies of the atomic pair in the large interatomic distance from  $980a_0$  to  $1000a_0$ . Black, red, blue, pink, and green lines denote the rotational potential curves for rotational quantum numbers  $l = 1, 2, 93, 94,$  and  $95$ , respectively.

with  $T_\omega = 100$  ps.

The initial-state distribution at thermal equilibrium can be described by the initial density operator

$$\hat{\rho}^T(t_0) = \frac{1}{Z} e^{-\beta \hat{H}_g}, \quad (7)$$

with

$$\hat{H}_g = \hat{T} + V_{X^1\Sigma_g^+}(R) + \frac{l(l+1)\hbar^2}{2\mu_m R^2}, \quad (8)$$

where  $\beta = 1/(k_B T)$ , with  $k_B$  being the Boltzmann constant and  $T$  the temperature.  $Z = \text{Tr}[e^{-\beta \hat{H}_g}]$  is the partition function and  $\hat{H}_g$  the ground-state Hamiltonian. The eigenfunction  $\psi_{nlm}$  of  $\hat{H}_g$  can be used to represent the basis function of the density operator, as done in Ref. [33]. The eigenfunction  $\psi_{nlm}$  is obtained by diagonalizing  $\hat{H}_g$  on a grid (for each  $l$ ), where  $n, l$ , and  $m$  label translational, rotational, and magnetic quantum numbers, respectively. The translational part of the eigenfunction contains the scattering and bound states. The sum over the magnetic quantum states yields a degeneracy factor  $(2l+1)/4\pi$ . The eigenfunction is now simplified as  $\psi_{nl}$ , corresponding to eigenvalue  $E_{nl}$ . Thus the initial density operator can be written as

$$\hat{\rho}^T(t_0) = \frac{1}{4\pi} \frac{1}{Z} \sum_{nl} (2l+1) e^{-\beta E_{nl}} |\psi_{nl}\rangle \langle \psi_{nl}|, \quad (9)$$

TABLE I. Rotational potential energies and unnormalized Boltzmann weights  $W_{R_{\max}}(l)$  for different  $l$ 's (from 1 to 95) at the largest interatomic distance,  $R_{\max} = 1000a_0$ .

$l$	$l(l+1)\hbar^2/2\mu_m R_{\max}^2$ (cm $^{-1}$ )	$W_{R_{\max}}(l)$
1	$2.835 \times 10^{-6}$	2.994
2	$8.507 \times 10^{-6}$	4.969
—	—	—
94	$1.266 \times 10^{-2}$	$2.091 \times 10^{-2}$
95	$1.293 \times 10^{-2}$	$1.741 \times 10^{-2}$

with

$$Z = \frac{1}{4\pi} \sum_{nl} (2l+1) e^{-\beta E_{nl}}. \quad (10)$$

The population in the excited electronic state after propagation of the eigenstate  $|\psi_{nl}\rangle$  from initial time  $t_0$  to final time  $t_f$  is given by

$$P_e^{nl}(t_f) = \sum_{v'l'_e} P_{v'l'_e}^{nl}(t_f), \quad (11)$$

$$P_{v'l'_e}^{nl}(t_f) = |\langle \psi_{v'l'_e} | \hat{U}(t_f, t_0) | \psi_{nl} \rangle|^2, \quad (12)$$

where  $\hat{U}(t_f, t_0)$  is the time-evolution operator.  $P_{v'l'_e}^{nl}(t_f)$  is the population in the rovibrational state  $|\psi_{v'l'_e}\rangle$  after propagation of eigenstate  $|\psi_{nl}\rangle$  from initial time  $t_0$  to final time  $t_f$ . The thermally averaged photoassociation probability is given by

$$P_{\text{TA}} = \sum_{nl} W_{nl} P_e^{nl}, \quad (13)$$

where

$$W_{nl} = \frac{(2l+1) e^{-\beta E_{nl}}}{\sum_{n'l'} (2l'+1) e^{-\beta E_{n'l'}}}, \quad (14)$$

is the weight of  $|\psi_{nl}\rangle$ . The weight depends on the degeneracy factor  $(2l+1)/4\pi$  and energy level distribution factor  $e^{-\beta E_{nl}}$ . The sum over the translational  $n$  and rotational  $l$  quantum numbers is cut off by the Boltzmann weight.

### III. RESULTS AND DISCUSSION

In our calculation, the spectral phase and the peak intensity of the laser pulse are taken to be 0 and  $2.5 \times 10^6$  W/cm $^2$ , respectively. In order to cover more vibrational levels of the excited electronic state, the FWHM of the laser pulse in the frequency domain is taken to be  $\omega_f = 2.0$  cm $^{-1}$ . The evolution time is taken to be 100 ps, with a step size of 0.01 ps, which is much shorter than the lifetimes of the  $^{85}\text{Rb}(5p^2 P_{1/2}, 5p^2 P_{3/2})$  levels and the excited electronic  $0_u^+$  state of the  $^{85}\text{Rb}_2$  molecule. Thus the spontaneous emission can be ignored.

The range of interatomic distance is taken to be  $[5a_0, 1000a_0]$  ( $a_0$  is the Bohr radius). For such a long box, the lowest scattering level with energy  $\propto \frac{1}{R_{\max}^2}$  is of the order of  $10^{-6}$  K. Therefore discretization of the continuum states is suitable for an energy of the millikelvin order. The sum over the rotational quantum number  $l$  in Eq. (5) is cut off by

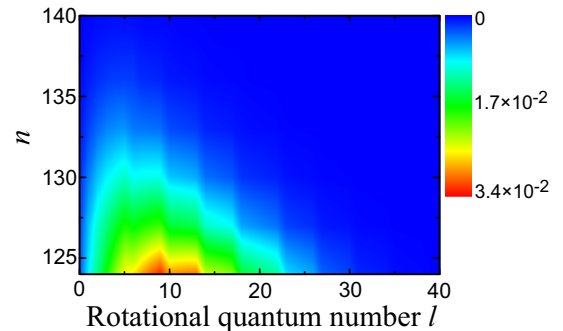


FIG. 3. Weight  $W_{nl}$  of  $|\psi_{nl}\rangle$  versus  $n$  and  $l$  at  $T = 2$  mK.

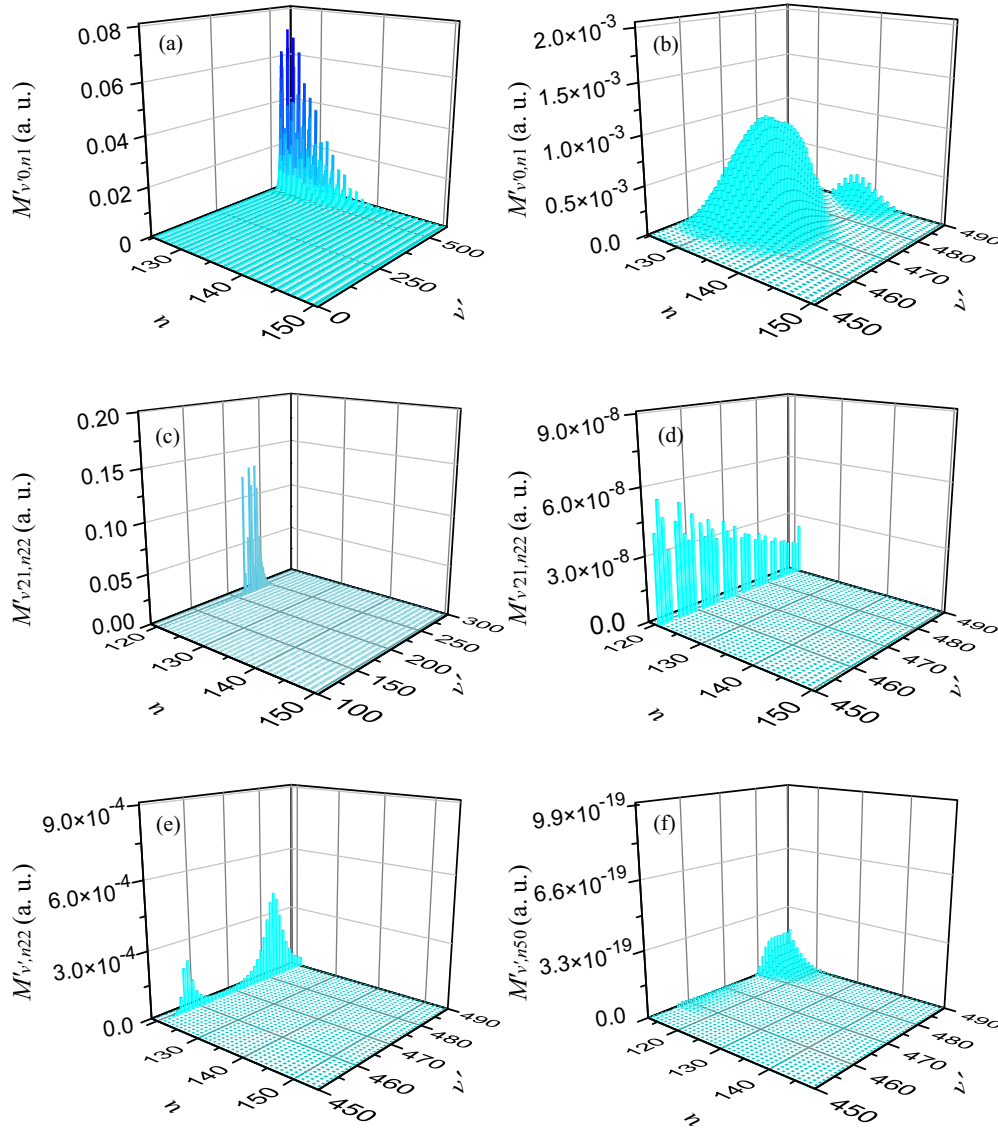


FIG. 4. Weighted transition matrix elements  $M'_{v'l_e, nl}$  between  $|\psi_{nl}\rangle$  and  $|\psi_{v'l_e}\rangle$ . (a)  $l = 1$ ,  $n = 124$ – $150$ ,  $l_e = 0$ , and  $v' = 0$ – $550$ . (b)  $l = 1$ ,  $n = 124$ – $150$ ,  $l_e = 0$ , and  $v' = 450$ – $490$ . (c)  $l = 22$ ,  $n = 118$ – $150$ ,  $l_e = 21$ , and  $v' = 100$ – $300$ . (d)  $l = 22$ ,  $n = 118$ – $150$ ,  $l_e = 21$ , and  $v' = 450$ – $490$ . (e)  $l = 22$ ,  $n = 118$ – $155$ , and  $v' = 450$ – $490$ . (f)  $l = 50$ ,  $n = 112$ – $148$ , and  $v' = 450$ – $490$ . In (e) and (f), the excited electronic state does not include the rotational structure  $l_e$ .

the Boltzmann weight. Figure 2 shows the rotational potential energies of the atomic pair at a large interatomic distance, from  $980a_0$  to  $1000a_0$ . The rotational potential energy increases with an increase in the rotational quantum number  $l$ . Table I lists the rotational potential energies  $l(l+1)\hbar^2/2\mu_m R_{\max}^2$  for  $l = 1$ – $95$  and their unnormalized Boltzmann weights  $W_{R_{\max}}(l)$  at the largest interatomic distance  $R_{\max}$  (here  $R_{\max}$  is taken to be  $1000a_0$ ). The unnormalized Boltzmann weight is given by

$$W_{R_{\max}}(l) = (2l+1)\exp\left[-\beta\frac{l(l+1)\hbar^2}{2\mu_m R^2}\right]. \quad (15)$$

At  $R_{\max}$ , the unnormalized Boltzmann weight  $W_{R_{\max}}(l)$  of the lowest scattering energy for the highest rotational quantum number  $l_{\max}$  must be small enough to be ignored. In Table I, the maximum rotational quantum number is taken to be  $l_{\max} = 95$ ,

which satisfies the requirement of an unnormalized Boltzmann weight  $W_{R_{\max}}(l_{\max}) < 0.02$  [33].

The weight  $W_{nl}$  and the excited-electronic-state population  $P_e^{nl}$  are two decisive factors for  $P_{TA}$ . Figure 3 shows the weight  $W_{nl}$  of  $|\psi_{nl}\rangle$  in the ranges of  $l = 0$ – $40$  and  $n = 124$ – $140$  at temperature  $T = 2$  mK. The translational part  $n$  of the eigenfunction contains the scattering and bound states.  $n = 124$  corresponds to the first scattering state for  $l = 0$ . Both the degeneracy factor  $(2l+1)/4\pi$  and the energy level distribution factor  $e^{-\beta E_{nl}}$  determine the distribution of the  $W_{nl}$ . In other words, the degeneracy of microscopic quantum states and the system temperature determine the distribution of the  $W_{nl}$ . The weight  $W_{nl}$  is mostly distributed in the ranges of  $l = 0$ – $35$  and  $n = 124$ – $138$ , as shown in Fig. 3. The weight  $W_{nl}$  outside this range is very low.

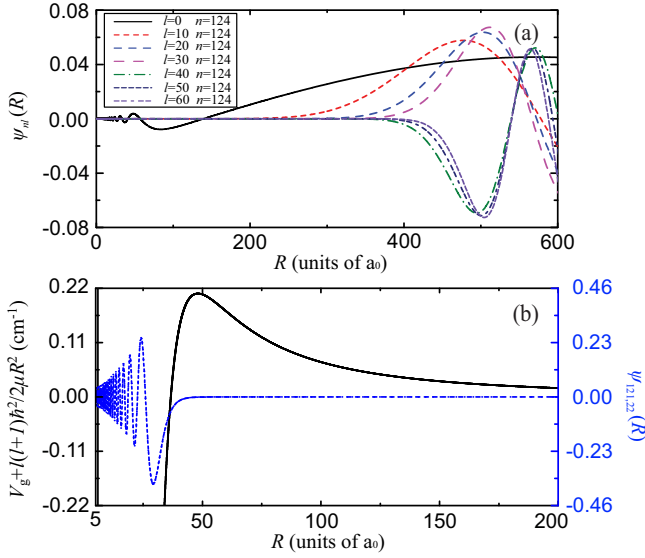


FIG. 5. (a) Wave functions  $\psi_{nl}$  versus  $R$  for  $n = 124$  and  $l = 0, 10, 20, 30, 40, 50,$  and  $60$ . (b) Wave function  $\psi_{121,22}$  (dashed blue line) for the collisional energy of 2.7 mK and the potential  $V_g + l(l+1)\hbar^2/2\mu R^2$  (solid black line) with  $l = 22$ .

The population  $P_e^{nl}$  is mainly determined by the transition matrix elements

$$M_{v'l_e, nl} = |\langle \psi_{v'l_e} | \mu(R) | \psi_{nl} \rangle|^2, \quad (16)$$

where  $|\psi_{v'l_e}\rangle$  are the  $v'$ th and the  $l_e$ th rovibrational state of the excited electronic state. Due to the thermodynamics effect, the weights of different eigenvalues  $E_{nl}$  are different. Thus, the Boltzmann weight should be taken into account in the transition matrix elements. The weighted transition matrix element is given by

$$M'_{v'l_e, nl} = \frac{e^{-\beta E_{nl}}}{\sum_{n'} e^{-\beta E_{n'l'}}} |\langle \psi_{v'l_e} | \mu(R) | \psi_{nl} \rangle|^2. \quad (17)$$

Figure 4 shows the weighted transition matrix elements between  $|\psi_{nl}\rangle$  and  $|\psi_{v'l_e}\rangle$ . The weighted transition matrix elements for  $l = 1, n = 124-150, l_e = 0,$  and  $v' = 0-550$  are shown in Fig. 4(a). Figure 4(b) displays the partially enlarged details for  $l = 1, n = 124-150, l_e = 0,$  and  $v' = 450-490$ . The central frequency  $\omega_0$  of the laser field is resonant with the vibrational level  $v' = 475$  of the excited electronic state, which corresponds to the largest transition matrix element  $M'_{v'=475, l_e=0, n=1}$  in the range of  $v' = 450-490$ . Figure 4(c) displays the weighted transition matrix elements for  $l = 22, n = 118-155, l_e = 0,$  and  $v' = 450-490$ . The weighted transition matrix elements between  $|\psi_{121,22}\rangle$  and  $|\psi_{v',21}\rangle$  are much larger than others in Fig. 4(c). Figure 4(d) shows the weighted transition matrix elements for  $l = 22, n = 118-150, l_e = 21,$  and  $v' = 450-490$ . The increase in the weighted transition matrix element results mainly from the shape resonance in the atomic scattering at the collision energy  $E = 2.7$  mK. In Figs. 4(e) and 4(f) the excited electronic state does not include the rotational structures  $l_e$ . The difference between Fig. 4(d) and Fig. 4(e) results from the rotational structure of the excited

electronic state. The weighted transition matrix element is very small for higher  $l$ , as shown in Fig. 4(f).

Since the rotational potential barrier of the ground electronic state decreases with a decrease in  $l$ , the wave-function amplitude with a lower rotational quantum number is lower than that with a higher one when  $R < 200a_0$ , as shown in Fig. 5(a). In the meantime, the wave function  $\psi_{v'l_e}$  is densely distributed in the range of a short interatomic distance. Therefore, the weighted transition matrix element for a lower rotational quantum number  $l$  is larger than that for a higher one. Figure 5(b) shows the wave function  $\psi_{n=121, l=22}$  for the collisional energy of 2.7 mK and the potential  $V_g + l(l+1)\hbar^2/2\mu R^2$  with  $l = 22$ . In Fig. 5(b), the wave function  $\psi_{n=121, l=22}$  is mostly distributed at a short interatomic distance, behind the rotational barrier. This phenomenon reflects the existence of a shape resonance, which leads to an increase in the weighted transition matrix element.

We first consider a simple case in which the rotational structure of the excited electronic state is not included in the calculation. Figure 6(a) shows the contribution of rotational state  $l$  to the  $P_{TA}$ :

$$P_e^l = \sum_n (2l+1) e^{-\beta E_{nl}} P_e^{nl}. \quad (18)$$

In Fig. 6(a), the population is mostly distributed in the range of lower rotational quantum numbers  $l_e \leq 8$ . This phenomenon also occurred in several experiments [34,44]. Several shape resonance positions are found in our calculation. The contribution of the rotational state  $l = 22$  to the  $P_{TA}$  is significantly enhanced due to the shape resonance at the collisional energy of  $E = 2.7$  mK. The increase in the transition probability stems from a large increase in the wave-function amplitude behind the rotational barrier. At  $T = 2.0$  mK, the energy range  $[0, 3.857 \times 10^{-3}]$  cm $^{-1}$  in which the initial thermal state is mostly distributed ( $W_{nl} \geq 5.022 \times 10^{-8}$ ) is fully contained within the bandwidth 2.0 cm $^{-1}$  of the laser pulse. In other words, the large bandwidth enables more rovibrational components of the initial thermal mixed state to participate in the photoassociation. There is more than one shape resonance in this range. Because of the shape resonances, the contributions of the rotational state  $l = 10, 14,$  and  $18$  to the  $P_{TA}$  are also enhanced. The collisional energies in shape resonances for  $l = 10, 14,$  and  $18$  are  $E = 10.1, 13.0,$  and  $10.9$  mK, respectively. Because of the high collisional energies at these resonances, their weights are very low. Therefore, their contributions to the  $P_{TA}$  are very small.

We now consider a general case in which the rotational structure of the excited electronic state is included in the calculation. Because the population is mostly distributed in the range of lower rotational quantum numbers  $l$ , the calculation should include relevant rotational states,  $l_e = 0-9$ , of the excited electronic state. The rotational state  $l = 22$  is not included in the calculation since  $M'_{v'21, n22}$  and  $M'_{v'23, n22}$  are very small in the range of  $v' = 450-490$ . If the target state is taken to be  $|\psi_{v'=200-250, l_e=21}\rangle$  or  $|\psi_{v'=200-250, l_e=23}\rangle$ , the contribution of rotational state  $l = 22$  to the  $P_{TA}$  will be significantly enhanced due to the shape resonance. Figure 6(b) displays the contribution of the excited rotational state  $l_e$  to the  $P_{TA}$  at

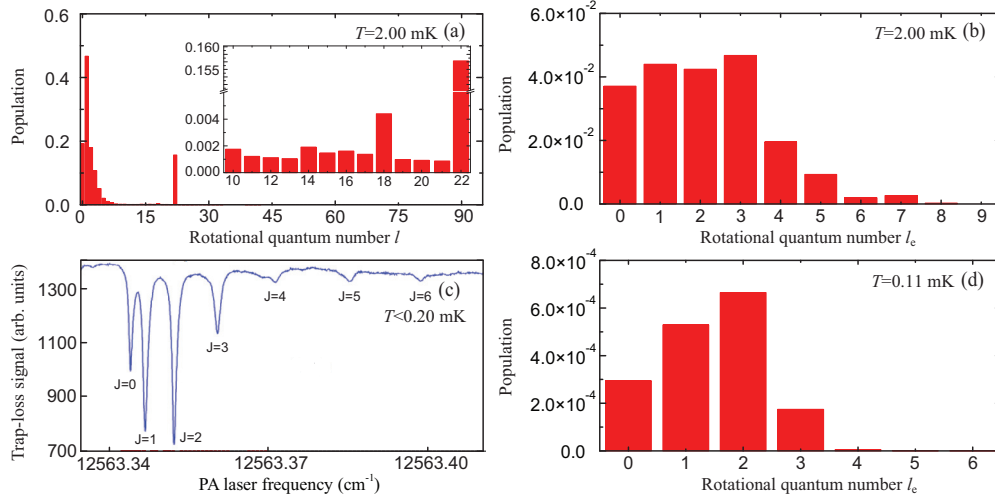


FIG. 6. (a) Unnormalized populations  $P_e^l$  for different rotational quantum numbers  $l$  at temperature  $T = 2$  mK. Inset: Partially enlarged detail from  $l = 10$  to  $l = 22$ . The calculation of the evolution process does not include the rotational structure of the excited electronic state. (b) Unnormalized population  $P_{l_e}$  for different rotational quantum numbers  $l_e$  at  $T = 2$  mK. The calculation of the evolution process includes the rotational structure of the excited electronic state. (c) Rotationally resolved trap-loss spectra for cw laser transitions to the  $0_u^+$  state [44], where the temperature is less than 0.20 mK. (d) Unnormalized population  $P_{l_e}$  for rotational quantum numbers  $l_e = 0-6$  at  $T = 0.11$  mK.

temperature  $T = 2$  mK:

$$P_{l_e} = \sum_{nl} \sum_{v'} P_{v'l_e}^{nl} W_{nl}. \quad (19)$$

The thermally averaged photoassociation probability  $P_{\text{TA}}$  is  $2.525 \times 10^{-4}$  at  $T = 2$  mK. In Fig. 6(b), the population is mostly distributed in the range of lower  $l_e$ . The maximal contribution to the  $P_{\text{TA}}$  comes from  $l_e = 3$ . When  $l_e \geq 4$ , the population starts to decrease significantly. When  $l_e = 9$ , the population is close to 0. This is because the weighted transition matrix element is very small when  $l_e \geq 8$ . We then compare the calculated  $P_{l_e}$  with the experimental results. Figure 6(c) shows rotationally resolved trap-loss spectra for cw laser transitions to the  $0_u^+$  state [34], where the temperature is less than 0.2 mK. Figure 6(d) shows the unnormalized population  $P_{l_e}$  for rotational quantum numbers  $l_e = 0-6$  at temperature  $T = 0.11$  mK. The calculated thermal weighted population distribution of excited rotational states agrees well with the photoassociation spectrum experiment.

Figure 7(a) shows the  $P_{\text{TA}}$  versus temperature. The change in the  $P_{\text{TA}}$  is mainly affected by the weight. Figures 7(d)–7(f) show the weights  $W_{nl}$  at  $T = 1.0, 1.5,$  and  $2.0$  mK. The weight  $W_{nl}$  is mostly distributed in the ranges of ( $n < 133, l < 25$ ), ( $n < 135, l < 30$ ), and ( $n < 138, l < 35$ ) at  $T = 1.0, 1.5,$  and  $2.0$  mK, respectively. Figure 7(b) shows the partition function  $Z(l) = \sum_{l'=0}^l \sum_n (2l'+1)e^{-\beta E_{nl}}$  versus the rotational quantum number  $l$ . It can be seen that the partition function converges very quickly with the increase in  $l$ . This rapid convergence is due to the dramatic rise in the centrifugal barrier height. The convergence of the partition function speeds up with the decrease in temperature, indicating that at low temperatures atomic collisions in the high rotational state are suppressed. Figure 7(c) shows the change in the partition function  $Z_l = \sum_n (2l+1)e^{-\beta E_{nl}}$  with  $l$ . As the temperature drops, the distribution of  $Z_l$  is concentrated in the range of lower rotational quantum numbers. By considering the overall

effects of  $Z$  and  $Z_l$ , the weight is concentrated in the range of lower  $n$  and  $l$  when the temperature decreases, as shown in Figs. 7(d)–7(f). In the meantime, the weighted transition matrix elements for lower translational and rotational quantum numbers are larger than those for higher ones. Therefore,  $P_{\text{TA}}$  decreases with an increase in temperature.

#### IV. CONCLUSION

In this paper, we have investigated theoretically the photoassociation process of  $^{85}\text{Rb}$  atoms driven by a short laser pulse at several millikelvins. At this temperature, some higher rotational and vibrational degrees of freedom for the initial scattering state and the excited electronic state are activated. The rotational barrier, the weight, and the shape resonance have an obvious influence on the photoassociation probability. The initial scattering state is described by the translational and the rotational quantum states with a Boltzmann distribution for colliding atoms, and the excited electronic state of the photoassociated molecule includes the vibrational and rotational degrees of freedom. The weight  $W_{nl}$  and the excited-electronic-state population  $P_{v'l_e}^{nl}$  are two decisive factors for enhancing the thermally averaged photoassociation probability  $P_{\text{TA}}$ . The weight  $W_{nl}$  is mostly distributed in the ranges of ( $n < 133, l < 25$ ), ( $n < 135, l < 30$ ), and ( $n < 138, l < 35$ ) at  $T = 1.0, 1.5,$  and  $2.0$  mK, respectively. At temperature  $T = 2.0$  mK, the rotational-state population  $P_{l_e}$  of the excited electronic state is mostly distributed in the range of  $l_e \leq 8$ . The population  $P_{l_e}$  reaches its maximal value when  $l_e = 3$  and is close to 0 when  $l_e \geq 9$ . The calculated thermal weighted population distribution of excited rotational states agrees well with the photoassociation spectrum experiment. The thermally averaged photoassociation probability decreases with rising temperature because the weight is concentrated in the range of lower  $n$  and  $l$  as the temperature drops.

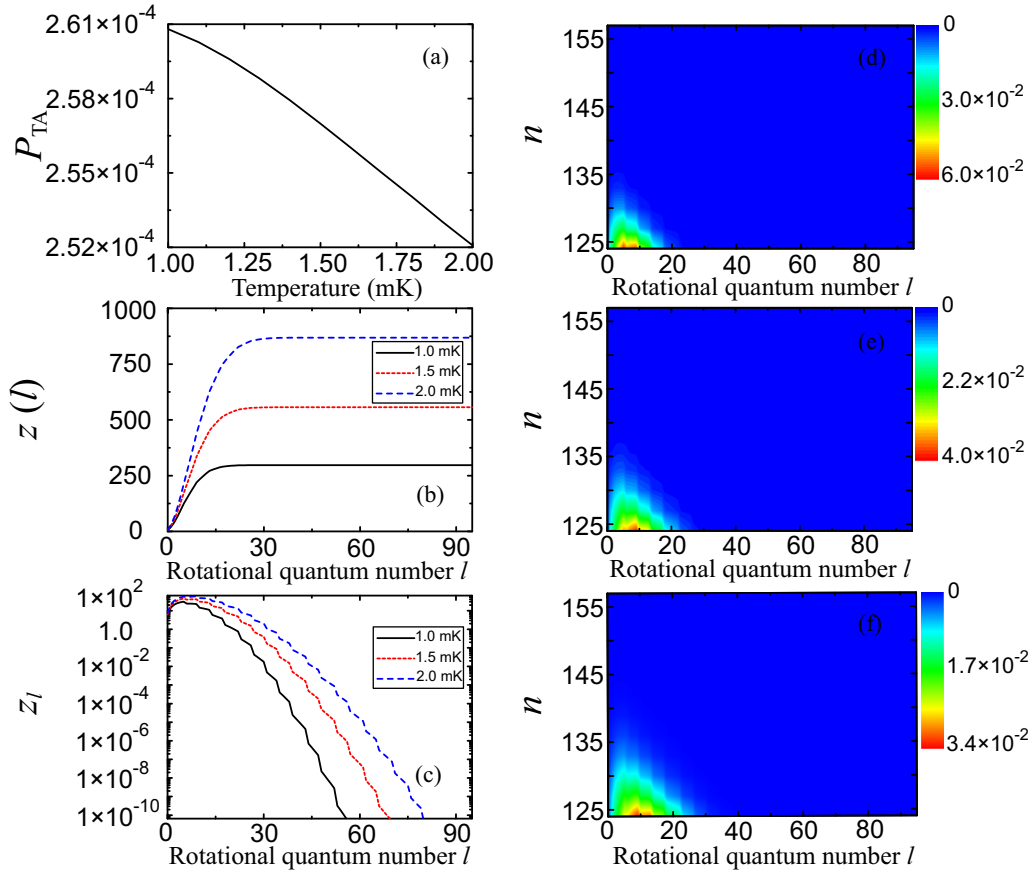


FIG. 7. (a)  $P_{TA}$  versus temperature. (b) Partition function  $Z(l) = \sum_{l'=0}^l \sum_n (2l' + 1) e^{-\beta E_{nl'}}$  as a function of rotational quantum number  $l$ . (c) Contribution of the rotational state  $l$  to the partition function  $Z_l = \sum_n (2l + 1) e^{-\beta E_{nl}}$ . (d–f) Weights  $W_{nl}$  at temperatures 1.0, 1.5, and 2.0 mK, respectively.

#### ACKNOWLEDGMENT

This work was supported by the National Natural Science Foundation of China under Grant No. 11274056.

- 
- [1] A. Micheli, G. K. Brennen, and P. Zoller, *Nat. Phys.* **2**, 341 (2006).
- [2] D. DeMille, *Phys. Rev. Lett.* **88**, 067901 (2002).
- [3] P. Rabl, D. DeMille, J. M. Doyle, M. D. Lukin, R. J. Schoelkopf, and P. Zoller, *Phys. Rev. Lett.* **97**, 033003 (2006).
- [4] E. R. Hudson, H. J. Lewandowski, B. C. Sawyer, and J. Ye, *Phys. Rev. Lett.* **96**, 143004 (2006).
- [5] T. Zelevinsky, S. Kotochigova, and J. Ye, *Phys. Rev. Lett.* **100**, 043201 (2008).
- [6] R. V. Krems, *Int. Rev. Phys. Chem.* **24**, 99 (2005).
- [7] C. Chin, R. Grimm, P. Julienne, and Tiesinga, *Rev. Mod. Phys.* **82**, 1225 (2010).
- [8] X. J. Hu, J. L. Li, T. Xie, Y. C. Han, and S. L. Cong, *Phys. Rev. A* **92**, 032709 (2015).
- [9] M. E. Wagshul, K. Helmerson, P. D. Lett, S. L. Rolston, W. D. Phillips, R. Heather, and P. S. Julienne, *Phys. Rev. Lett.* **70**, 2074 (1993).
- [10] J. D. Miller, R. A. Cline, and D. J. Heinzen, *Phys. Rev. Lett.* **71**, 2204 (1993).
- [11] A. Fioretti, D. Comparat, A. Crubellier, O. Dulieu, F. Masnou-Seeuws, and P. Pillet, *Phys. Rev. Lett.* **80**, 4402 (1998).
- [12] A. J. Kerman, J. M. Sage, S. Sainis, T. Bergeman, and D. DeMille, *Phys. Rev. Lett.* **92**, 153001 (2004).
- [13] J. Ulmanis, J. Deiglmayr, M. Repp, R. Wester, and M. Weidemüller, *Chem. Rev.* **112**, 4890 (2012).
- [14] J. Weiner, V. S. Bagnato, S. Zilio, and P. S. Julienne, *Rev. Mod. Phys.* **71**, 1 (1999).
- [15] F. Masnou-Seeuws and P. Pillet, *Adv. At. Mol. Opt. Phys.* **47**, 53 (2001).
- [16] A. M. Weiner, *Rev. Sci. Instrum.* **71**, 1929 (2000).
- [17] A. M. Weiner, *Opt. Commun.* **284**, 3669 (2011).
- [18] E. Luc-Koenig, R. Kosloff, F. Masnou-Seeuws, and M. Vatasescu, *Phys. Rev. A* **70**, 033414 (2004).
- [19] C. P. Koch, E. Luc-Koenig, and F. Masnou-Seeuws, *Phys. Rev. A* **73**, 033408 (2006).
- [20] M. J. Wright, J. A. Pechkis, J. L. Carini, S. Kallush, R. Kosloff, and P. L. Gould, *Phys. Rev. A* **75**, 051401 (2007).

- [21] W. Zhang, Y. Huang, T. Xie, G. R. Wang, and S. L. Cong, *Phys. Rev. A* **82**, 063411 (2010).
- [22] L. Levin, W. Skomorowski, L. Rybak, R. Kosloff, C. P. Koch, and Z. Amitay, *Phys. Rev. Lett.* **114**, 233003 (2015).
- [23] B. J. Lester, N. Luick, A. M. Kaufman, C. M. Reynolds, and C. A. Regal, *Phys. Rev. Lett.* **115**, 073003 (2015).
- [24] M. Gacesa, S. Ghosal, J. N. Byrd, and R. Côté, *Phys. Rev. A* **88**, 063418 (2013).
- [25] H. M. J. M. Boesten, C. C. Tsai, B. J. Verhaar, and D. J. Heinzen, *Phys. Rev. Lett.* **77**, 5194 (1996).
- [26] R. González-Férez and C. P. Koch, *Phys. Rev. A* **86**, 063420 (2012).
- [27] M. A. Bellos, R. Carollo, D. Rahmlow, J. Banerjee, E. E. Eyler, P. L. Gould, and W. C. Stwalley, *Phys. Rev. A* **86**, 033407 (2012).
- [28] K. Sakimoto, *Phys. Rev. A* **94**, 042701 (2016).
- [29] W. Skomorowski, Y. Shagam, E. Narevicius, and C. P. Koch, *J. Phys. Chem. A* **120**, 3309 (2016).
- [30] K. M. Jones, E. Tiesinga, P. D. Lett, and P. S. Julienne, *Rev. Mod. Phys.* **78**, 483 (2006).
- [31] Y. Huang, W. Zhang, G. R. Wang, T. Xie, and S. L. Cong, *Phys. Rev. A* **86**, 043420 (2012).
- [32] S. Amaran, R. Kosloff, M. Tomza, W. Skomorowski, F. Pawłowski *et al.*, *J. Chem. Phys.* **139**, 164124 (2013).
- [33] C. P. Koch, R. Kosloff, E. Luc-Koenig, F. Masnou-Seeuws, and A. Crubellier, *J. Phys. B* **39**, S1017 (2006).
- [34] J. R. Gardner, R. A. Cline, J. D. Miller, D. J. Heinzen, H. M. J. M. Boesten, and B. J. Verhaar, *Phys. Rev. Lett.* **74**, 3764 (1995).
- [35] J. Y. Seto, R. J. Le Roy, J. Vergès, and C. Amiot, *J. Chem. Phys.* **113**, 3067 (2000).
- [36] T. Bergeman, J. Qi, D. Wang, Y. Huang, H. K. Pechkis, E. E. Eyler, P. L. Gould, W. C. Stwalley, R. A. Cline, J. D. Miller, and D. J. Heinzen, *J. Phys. B* **39**, S813 (2006).
- [37] R. Beuc, M. Movre, V. Horvatic, C. Vadla, O. Dulieu, and M. Aymar, *Phys. Rev. A* **75**, 032512 (2007).
- [38] K. Willner, O. Dulieu, and F. Masnou-Seeuws, *J. Chem. Phys.* **120**, 548 (2004).
- [39] H. Tal-Ezer and R. Kosloff, *J. Chem. Phys.* **81**, 3967 (1984).
- [40] R. Kosloff, *J. Phys. Chem.* **92**, 2087 (1988).
- [41] A. Monmayrant, S. Weber, and B. Chatel, *J. Phys. B* **43**, 103001 (2010).
- [42] K. Hoki, Y. Ohtsuki, H. Kono, and Y. Fujimura, *J. Phys. Chem. A* **103**, 6301 (1999).
- [43] C. C. Shu and N. E. Henriksen, *J. Chem. Phys.* **134**, 164308 (2011).
- [44] Y. Huang, J. Qi, H. K. Pechkis, D. Wang, E. E. Eyler, P. L. Gould, and W. C. Stwalley, *J. Phys. B* **39**, S857 (2006).